



HAL
open science

Clinical relevance of augmented statistical shape model of the scapula in the glenoid region

Asma Salhi, Valérie Burdin, Sylvain Brochard, Tinashe Mutsvangwa, Bhushan
Borotikar

► **To cite this version:**

Asma Salhi, Valérie Burdin, Sylvain Brochard, Tinashe Mutsvangwa, Bhushan Borotikar. Clinical relevance of augmented statistical shape model of the scapula in the glenoid region. *Medical Engineering & Physics*, 2020, 76 (1), pp.88-94. 10.1016/j.medengphy.2019.11.007 . hal-02448027

HAL Id: hal-02448027

<https://imt-atlantique.hal.science/hal-02448027>

Submitted on 21 Jul 2022

HAL is a multi-disciplinary open access archive for the deposit and dissemination of scientific research documents, whether they are published or not. The documents may come from teaching and research institutions in France or abroad, or from public or private research centers.

L'archive ouverte pluridisciplinaire **HAL**, est destinée au dépôt et à la diffusion de documents scientifiques de niveau recherche, publiés ou non, émanant des établissements d'enseignement et de recherche français ou étrangers, des laboratoires publics ou privés.



Distributed under a Creative Commons Attribution - NonCommercial 4.0 International License

1 **Clinical relevance of augmented statistical** 2 **shape model of the scapula in the glenoid** 3 **region**

4 Asma Salhi^{1,2}, Valérie Burdin^{1,2}, Sylvain Brochard^{1,3,4}, Tinashe E. Mutsvangwa⁵, Bhushan
5 Borotikar^{1,3,4}

6 ¹ *Laboratoire de Traitement de l'Information Médicale (LaTIM), INSERM U1101, Brest, France*

7
8 ² *Département Image et traitement de l'information, IMT Atlantique, Brest, France*

9
10 ³ *CHRU de Brest, Hôpital Morvan, Brest, France*

11
12 ⁴ *University of Western Brittany, Brest, France*

13
14 ⁵ *Division of Biomedical Engineering, University of Cape Town, Cape Town, South Africa*

15

16

17 **Running Title:** *Clinical relevance of augmented scapula SSM*

18 **Manuscript:** Total 2398 words (not including references) with 3 figures and 4 tables.

19

20 **Corresponding Author**

21 Bhushan Borotikar, MBA, D.Eng.

22

23 Laboratory for Medical Information Processing (LaTIM), INSERM UMR 1101

24 <http://latim.univ-brest.fr/>

25 Faculte de Medicine, Batiment E- IBRS, 1ere etage

26 22, Ave. Camille Desmoulins

27 C.S. 93837 - 29238, Brest, Cedex - 3

28 Phone 02 98 01 81 05 / Fax: 02 98 01 81 24

29 E-mail: phdfile@gmail.com

30

31 **ABSTRACT**

32 Objective: To illustrate a) whether a statistical shape model (SSM) augmented with anatomical
33 landmark set(s) performs better fitting and provides improved clinical relevance over non-
34 augmented SSM and b) which anatomical landmark set provides the best augmentation strategy
35 for predicting the glenoid region of the scapula. Methods: Scapula SSM was built using 27 dry
36 bone CT scans and augmented with three anatomical landmark sets (16 landmarks each)
37 resulting in three augmented SSMs ($aSSM_{\text{proposed}}$, $aSSM_{\text{set1}}$, $aSSM_{\text{set2}}$). The non-augmented and
38 three augmented SSMs were then used in a non-rigid registration (regression) algorithm to fit to
39 six external scapular shapes. The prediction error by each type of SSM was evaluated in the
40 glenoid region for the goodness of fit (mean error, root mean square error, Hausdorff distance
41 and Dice similarity coefficient) and for four anatomical angles (Critical shoulder angle, lateral
42 acromion angle, glenoid inclination, glenopolar angle) . Results: Inter- and Intra-observer
43 reliability for landmark selection was moderate to excellent ($ICC > 0.74$). Prediction error was
44 significantly lower for $SSM_{\text{non-augmented}}$ for mean (0.9mm) and root mean square (1.15mm)
45 distances. Dice coefficient was significantly higher (0.78) for $aSSM_{\text{proposed}}$ compared to all other
46 SSM types. Prediction error for anatomical angles was lowest using the $aSSM_{\text{proposed}}$ for critical
47 shoulder angle (3.4°), glenoid inclination (2.6°), and lateral acromion angle (3.2°). Conclusion
48 and Significance: The conventional SSM robustness criteria or better goodness of fit do not
49 guarantee improved anatomical angle accuracy which may be crucial for certain clinical
50 applications in pre-surgical planning. This study provides insights into how SSM augmented
51 with region-specific anatomical landmarks can provide improved clinical relevance.

52

53 **Keywords:** iterative closest point, SSM robustness, shoulder surgery, registration

54 **INTRODUCTION**

55 Statistical shape models (SSMs) describe an average shape distribution within a certain
56 population [1, 2]. SSMs provide a method to quantify the shape of an object using only a limited
57 number of parameters which then allows a three-dimensional (3D) morphometric analysis of an
58 object using automatic shape annotation. Such annotated models then can be effectively used in
59 computer-aided orthopedic surgeries [3-5] or in pre-surgical planning [6-8] for fitting the
60 patient's bone shape. Despite these facts, it is still not clear whether the use of such models has
61 improved clinical relevance in pre-surgical planning or treatment applications [9], specifically
62 for glenohumeral surgery planning.

63 For glenohumeral surgical procedures, surgeons typically rely on virtual palpations or anatomical
64 measures using medical images [10-14]. Recently, scapula SSMs are used in pre-surgery
65 planning to automatically determine anatomical measures of interest [15, 16]. However, SSMs
66 can be effective only if they can improve clinically relevant measures. For the glenoid region,
67 four anatomical angle measures are frequently associated with the clinical assessment of the
68 shoulder pathology and frequently referred to by surgeons and clinicians. These include Critical
69 shoulder angle (CSA) [17], Glenoid inclination [18], Lateral acromion angle [19], and
70 Glenopolar angle [20, 21]. The classic metrics used to evaluate the computational robustness of
71 the SSM (Specificity, generality, and compactness) [22, 23] do not necessarily guarantee the
72 desired accuracy in anatomical angle measurements that are clinically relevant [24].
73 Furthermore, shape fitting algorithms typically use a certain set of anatomical landmarks during
74 the fitting process without considering the clinical relevance or efficacy of using such landmarks
75 sets.

76 The objective of this study was to illustrate a) whether an SSM augmented with anatomical
77 landmarks performs better fitting and provides improved clinical relevance over non-augmented
78 SSM and b) which anatomical landmark sets provide best augmentation strategy. For the scope
79 of this study, two types of measures were evaluated 1) measure of the goodness of fit (three-
80 dimensional distance errors) for predicting the glenoid region of scapular bone, and 2) measure
81 of accuracy to predict the anatomical angles associated with this region. We hypothesize that a
82 categorical landmark selection process based on the glenoid region as a region of interest would
83 improve the clinical relevance of the scapular SSM in terms of goodness of fit and anatomical
84 angle predictions. Objectives of the study were achieved by comparing the use of non-augmented
85 SSM with three augmented SSMs for illustrating improvements in the two measures. One of the
86 three augmented SSMs was proposed earlier [6] but whether it improves the overall measures of
87 clinical relevance in surgical planning of the glenoid region was not reported.

88

89 **METHODS**

90 Thirty-three dry scapulae bones were acquired from a local hospital's anatomy department. CT
91 scans were acquired using the SIEMENS SOMATOM Definition AS scanner (Siemens
92 Healthcare, Forchheim, Germany) with a resolution of 0.96mm X 0.96mm X 0.6mm. A
93 radiologist checked all the images for any signs of trauma (exclusion criteria). A scapula SSM
94 built with a set of 27 bones using previously published IMCP-GMM (Iterative Median Closest
95 Point–Gaussian Mixture Model) methodology [6, 25] was adopted in this study. This SSM will
96 be referred to as $SSM_{\text{non-augmented}}$ throughout this study. Computational robustness of the $SSM_{\text{non-}}$
97 augmented has been reported earlier through the measures of generality, specificity, and

98 compactness [25]. Briefly, compactness measures dimensionality reduction and reports model's
99 ability to use as few shape parameters as possible to cover shape variability [23]. Generality
100 measures a model's ability to represent unseen instances of the class of object [23]. This property
101 highlights the capability of a model to fit to a new shape. Specificity measures the model's
102 ability to generate instances of the species of objects similar to those in the training set [23].

103

104 *Augmented SSM creation for comparisons*

105 To fulfill the objectives of the study, three augmented SSMs were created: $aSSM_{\text{proposed}}$,
106 $aSSM_{\text{set1}}$, $aSSM_{\text{set2}}$. To create an augmented SSM, the $SSM_{\text{non-augmented}}$ was supplemented with
107 additional set of 16 anatomical landmarks and their deformation field in the training dataset [6].
108 The $aSSM_{\text{proposed}}$ was augmented with a proposed set of 16 clinically relevant anatomical
109 landmarks to map scapular shape [6] with previously evaluated inter- and intra-observer
110 reliability for each landmark selection [6]. This landmark set consisted six anatomical landmarks
111 in the glenoid cavity region and four landmarks on the acromion region (Figure 1). To illustrate
112 the best augmentation strategy to improve fitting quality and clinical relevance, two more sets of
113 augmented SSMs ($aSSM_{\text{set1}}$ and $aSSM_{\text{set2}}$) having 16 anatomical landmarks each were created
114 (Figure 1). Specifically, $aSSM_{\text{set1}}$ landmarks were selected without considering the clinical
115 significance of their anatomical locations but covering the entire scapula shape (Figure 1). For
116 $aSSM_{\text{set2}}$, no anatomical landmarks were selected in the glenoid cavity region (as against six
117 landmarks in the $aSSM_{\text{proposed}}$ and three landmarks in $aSSM_{\text{set1}}$) (Figure 1).

118

119

INSERT Figure 1 about here

120 Inter- and intra-observer reliability analysis for anatomical landmark selection for set1 and set2
121 was performed on all 27 internal instances by two independent observers. For the intra-observer
122 reproducibility evaluation, each observer repeated the landmark selection process two times per
123 set. A time interval of 60 to 72 hours was allowed to expire between the trials while the order of
124 instance selection was also randomized. Inter-observer reliability was defined by ICC, using a
125 two-way mixed effects (choice of observers) analysis of variance (ANOVA) [26]. Intra-observer
126 reproducibility was also defined by ICCs, using a two way ANOVA and considering the choice
127 of the observer as fixed effects [26]. The standard error of measurement ($SEM = SD * \sqrt{1-ICC}$),
128 where SD is the standard deviation of the whole set of measures) was quantified for each set of
129 landmark measurements. All the ICCs were obtained using Statistica (StatSoft, Inc., Paris,
130 France).

131

132 ***Prediction error evaluation***

133 Prediction error was determined by fitting each of the augmented SSMs ($aSSM_{proposed}$, $aSSM_{set1}$,
134 and $aSSM_{set2}$) and $SSM_{non-augmented}$ to six external scapulae (not used in SSM building) and
135 comparing the predicted shape with the original shape (manually segmented from the CT scans)
136 for fitting quality and predicting anatomical angle measures in the glenoid region. The glenoid
137 region of the scapula was identified by cutting the scapula through its surgical neck as previously
138 described [27, 28]. The capability of $aSSM_{proposed}$ to fit to the glenoid region was compared with
139 $aSSM_{set1}$ and $aSSM_{set2}$ and $SSM_{non-augmented}$. A standard deformable model fitting algorithm (non-
140 rigid iterative closest point) [29] was created in SCALISMO, an open source toolbox for creating
141 and evaluating statistical shape algorithms [30]. The algorithm was performed in three steps: 1)
142 Matching the mesh centroids of the mean shape of each SSM type under evaluation with each of

143 the external scapular shape, 2) Rigid alignment of each SSM type to each of the external scapular
144 shapes using the set of landmarks and fifteen iterations of rigid iterative closest point algorithm
145 [31], and 3) one-time non-rigid regression (non-rigid iterative closest point algorithm) to non-
146 rigidly deform the rigidly aligned SSM to the external shape [31, 32].

147 Clinical relevance was individually sought in the measures of the goodness of fit and anatomical
148 angle predictions between the original glenoid region identified in the external scapulae and its
149 predicted counterpart. The goodness of fit was quantified using three distance measures (mean
150 distance, root mean square (RMS) distance, maximum (Hausdorff) distance [33]) and a similarity
151 measure (Dice coefficient). Four anatomical measures associated with glenoid region were also
152 selected. These include 1) Critical shoulder angle [34, 35], 2) Glenoid inclination [18], 3) Lateral
153 acromion angle [36], and 4) glenopolar angle [37]. Differences between the original scapular
154 shape and the predicted shape for each of the measures described above were first determined for
155 each SSM type and termed as the prediction error. Prediction error for distance measures
156 obtained from $SSM_{\text{non-augmented}}$, $aSSM_{\text{set1}}$, and $aSSM_{\text{set2}}$ was compared with $aSSM_{\text{proposed}}$ using
157 paired student's T-tests. Prediction error for anatomical angle measures was qualitatively
158 compared using absolute mean differences.

159 **RESULTS**

160 *Intra-observer reproducibility and inter-observer reliability*

161 Both the observers successfully completed the reliability tests for anatomical landmark selection
162 for both the sets ($aSSM_{\text{set1}}$, $aSSM_{\text{set2}}$). Moderate to excellent ($ICC > 0.73$) intra- and inter-
163 observer reliability was found for all X, Y and Z coordinates (Annexure I - Table 1, Table 3, and
164 Table 5). The ICC for inter-observer reliability ranged from 0.74 to 0.98 for all the coordinates

165 (Annexure I - Table 1). The ICC for intra-observer reproducibility for all the observers ranged
166 from 0.79 to 0.96 for all the coordinates (Annexure I - Table 3 and Table 5). The SEM ranged
167 from 0.05mm to 0.39mm for all intra- and inter-observer measurements (Annexure I – Table 2,
168 Table 4, Table 6).

169

INSERT Figure 2 about here

170

171 *Prediction error*

172 The fitting algorithm was able to successfully deform each of the SSMs to the six external
173 scapular shapes (Figure 2). Prediction error for all the distance measures (goodness of fit) was
174 significantly lower for $SSM_{non-augmented}$ than the three augmented SSMs (Figure 3) except for
175 Hausdorff distance. Dice coefficient was significantly higher (0.78) for $aSSM_{proposed}$ compared to
176 all other SSM types (Figure 3). Prediction error for anatomical angles was lowest using the
177 $aSSM_{proposed}$ for critical shoulder angle (3.4°), glenoid inclination (2.6°), and lateral acromion
178 angle (3.2°) (Table 1, Table 2, and Table 3). Whereas, for the glenopolar angle, the absolute
179 mean difference was lowest using $SSM_{non-augmented}$
180 (1.5°) (Table 4).

181

INSERT Figure 3 about here

182

183 **DISCUSSION**

184 This preliminary study highlighted the importance of using the scapula SSM augmented with
185 categorically selected anatomical landmarks for the glenoid region, in pre-surgery planning tools.

186 The results of this study reported that $SSM_{\text{non-augmented}}$ performed better in the goodness of fit
187 measures whereas $aSSM_{\text{proposed}}$ performed better in determining anatomical angle measures that
188 are clinically relevant. In doing so, this study also illustrated improvements in anatomical angle
189 predictions when mapping of the glenoid region by anatomical landmarks was increased
190 stepwise from landmark set 2 (no glenoid landmarks) to set 1 (three glenoid landmarks) and to
191 proposed set (six glenoid landmarks).

192 Results of ICCs for landmark selection achieved similar levels for all the three landmark sets,
193 which provided another indirect reliability measure. Also, both the reliability measures were
194 lower for landmarks that were not anatomically defined (landmarks 8, 10, and 15 in set1 or
195 landmarks 3, 5, 7, 9, and 10 in set2). Thus, we do not recommend selecting these landmarks
196 when creating an augmented SSM.

197 The significantly higher levels of goodness of fit measures using $SSM_{\text{non-augmented}}$ can be
198 attributed to the model fitting process. The non-rigid deformation step (step 3) was aimed at
199 finding the closest shape variation of the SSM to the target external shape. During this step, the
200 landmarks used for the rigid alignment in step 2 of the process were used to compute a
201 conditional distribution of the shape and subsequently build a posterior shape model that
202 represents the original SSM [38]. While using non augmented SSM, we can choose any or all
203 mesh points of the mean mesh of the $SSM_{\text{non-augmented}}$ to create this conditional distribution. For
204 the purpose of this study, we used all the mesh points to build the posterior model. Thus, the
205 overall goodness of fit (mean error, RMS error, Hausdorff distance, and Dice score) was better
206 using non-augmented SSM. However, as hypothesized, this goodness of fit did not necessarily
207 reflect higher accuracy in predicting the anatomical angle measures.

208 Anatomical angles quantified in this study have been previously reported to have clinical
209 relevance during surgery (or surgery-planning). Higher CSA and Glenoid inclination angle are
210 associated with osteoarthritis (OA) and rotator cuff tears and surgical aim is to reduce these
211 angles [17, 18]. Low lateral acromion angle is associated with full thickness supraspinatus tears
212 and surgical procedures avoid keeping this angle low post-surgery [19]. Glenohumeral
213 angulation deformities and shortening of the scapular neck are associated with scapular neck
214 fractures and assessed with glenopolar angle in AP radiographs [21, 37]. For the treatment of
215 extra-articular scapular neck fractures, most common recommendation is to keep glenopolar
216 angle less than 20° [20, 39, 40]. Results of prediction error in determining anatomical angle
217 measures highlighted higher performance of the $\alpha\text{SSM}_{\text{proposed}}$ while revealing a pattern of fitting.
218 For $\text{SSM}_{\text{non-augmented}}$, prediction errors were on both the negative and positive side of the original
219 angle value for all the angles. But for augmented SSMs, the glenoid inclination was almost
220 always overpredicted and the glenopolar angle was almost always underpredicted. This could be
221 attributed to the position of landmarks in the augmented SSMs constraining the fitting in these
222 regions and making it over or under predict.

223 State-of-the-art glenoid pre-surgery planning tools incorporate automatic 3D reconstruction of
224 medical images using scapula SSMs. The fitting algorithm uses intensity information or
225 landmark information derived from images. In these cases, anatomical landmarks play a crucial
226 role either by providing an initial alignment or generating a posterior model for a recursive
227 fitting algorithm. The objectives and results of this preliminary study do not intend to prove that
228 $\alpha\text{SSM}_{\text{proposed}}$ has sufficient accuracy for its use in a pre-surgical planning tool. However, it
229 provides a clear distinction and a necessary rationale and validation for not relying only on the

230 goodness of fit or SSM robustness (generality, specificity, compactness) measures when using
231 the SSM for pre-surgical planning.

232

233 This study posed certain limitations: 1) the sample sufficiency in building the scapula SSM with
234 27 dry bones was not evaluated, which could reflect in errors while fitting the SSM to new data.
235 2) prediction error and related clinical relevance was illustrated in only six external instances
236 which may not cover all the variations of the glenoid region. Thus, further evaluations in the
237 statistical stability of the SSM and completeness in terms of sample sufficiency are warranted.

238 **PERSPECTIVES AND CONCLUSIONS**

239 Evaluating the efficacy of the fitting algorithm was not in the scope of this study. Since similar
240 fitting algorithm and related parameters were used across the four SSM types in terms of
241 initiation, level of fitting, and the number of vertices, the fitting errors were deemed equal and
242 not affecting the analysis. Future efforts will be focused on enhancing the accuracy of fitting
243 algorithms. Furthermore, checking the accuracy of partial or missing data was not in the scope of
244 this paper, however, the augmented SSM would be used in this context in future studies. In
245 conclusion, the utility of SSM for its use in clinical applications is an under-evaluated problem.
246 The goodness of fit and prediction errors in anatomical measures reported in this study presents
247 the rationale of using augmented SSMs in the clinical setting and has a direct correlation with
248 clinical accuracy. This study also lays a foundation for the development of an accurate and
249 reliable methodology for the automatic segmentation of bone structures from medical images.

250 **ACKNOWLEDGEMENTS**

251 Competing interests: None declared. Funding: This research was supported by Bretagne region
252 grant 2015-2017 and Ph.D. funding during 2016-2019 was provided by Institut Carnot, France.
253 Ethical approval: Not required

254

255 REFERENCES

- 256 [1] Sarkalkan N, Waarsing JH, Bos PK, Weinans H, Zadpoor AA. Statistical shape and appearance models
257 for fast and automated estimation of proximal femur fracture load using 2D finite element models.
258 Journal of biomechanics. 2014;47:3107-14.
- 259 [2] Sarkalkan N, Weinans H, Zadpoor AA. Statistical shape and appearance models of bones. Bone.
260 2014;60:129-40.
- 261 [3] Batchelor GP, Edwards, P.J., King, A.P. 3D Medical Imaging. In: Pears N, Liu, Y., Bunting, P., editor. 3D
262 Imaging, Analysis and Applications. London: Springer-Verlag; 2012. p. 445-95.
- 263 [4] Pratt P, Mayer E, Vale J, Cohen D, Edwards E, Darzi A, et al. An effective visualisation and registration
264 system for image-guided robotic partial nephrectomy. J Robotic Surg. 2012;6:23-31.
- 265 [5] Stindel E, Briard JL, Merloz P, Plaweski S, Dubrana F, Lefevre C, et al. Bone morphing: 3D
266 morphological data for total knee arthroplasty. Computer aided surgery : official journal of the
267 International Society for Computer Aided Surgery. 2002;7:156-68.
- 268 [6] Borotikar B, Mutsvangwa T, Burdin V, Ghorbel E, Lempereur M, Brochard S, et al. Augmented
269 Statistical Shape Modeling for Orthopaedic Surgery and Rehabilitation. In: Azevedo-Marques; PMd,
270 Mencattini; A, Salmeri; M, Rangayyan RM, editors. Medical Image Analysis and Informatics: Computer-
271 Aided Diagnosis and Therapy. Florida, USA: CRC Press, Taylor and Francis Group; 2017. p. 369-426.
- 272 [7] Morooka Ki, Nakamoto M, Sato Y. A Survey on Statistical Modeling and Machine Learning
273 Approaches to Computer Assisted Medical Intervention: Intraoperative Anatomy Modeling and
274 Optimization of Interventional Procedures. IEICE Transactions on Information and Systems.
275 2013;E96.D:784-97.
- 276 [8] Vanden Berghe P, Demol J, Gelaude F, Vander Sloten J. Virtual anatomical reconstruction of large
277 acetabular bone defects using a statistical shape model. Computer methods in biomechanics and
278 biomedical engineering. 2017;20:577-86.

- 279 [9] Jan SVS. Introducing Anatomical and Physiological Accuracy in Computerized Anthropometry for
280 Increasing the Clinical Usefulness of Modeling Systems. 2005;17:249-74.
- 281 [10] Gomes G, Van Cauter, S., De. Beule, M., Vigneron, L., Pattyn, C., Audenaert, E. Patient-specific
282 modelling in orthopedics: from image to surgery. Lecture Notes in Computational Vision and
283 Biomechanics: Springer; 2013. p. 109-29.
- 284 [11] Boileau P, Cheval D, Gauci MO, Holzer N, Chaoui J, Walch G. Automated Three-Dimensional
285 Measurement of Glenoid Version and Inclination in Arthritic Shoulders. The Journal of bone and joint
286 surgery American volume. 2018;100:57-65.
- 287 [12] Frankle MA, Teramoto A, Luo Z-P, Levy JC, Pupello D. Glenoid morphology in reverse shoulder
288 arthroplasty: Classification and surgical implications. Journal of Shoulder and Elbow Surgery.
289 2009;18:874-85.
- 290 [13] Gupta A, Thussbas C, Koch M, Seebauer L. Management of glenoid bone defects with reverse
291 shoulder arthroplasty—surgical technique and clinical outcomes. Journal of Shoulder and Elbow Surgery.
292 2018;27:853-62.
- 293 [14] Walker KE, Simcock XC, Jun BJ, Iannotti JP, Ricchetti ET. Progression of Glenoid Morphology in
294 Glenohumeral Osteoarthritis. The Journal of bone and joint surgery American volume. 2018;100:49-56.
- 295 [15] Ablar D, Berger S, Terrier A, Becce F, Farron A, Buchler P. A statistical shape model to predict the
296 premorbid glenoid cavity. Journal of shoulder and elbow surgery / American Shoulder and Elbow
297 Surgeons [et al]. 2018;27:1800-8.
- 298 [16] Plessers K, Vanden Berghe P, Van Dijck C, Wirix-Speetjens R, Debeer P, Jonkers I, et al. Virtual
299 reconstruction of glenoid bone defects using a statistical shape model. Journal of shoulder and elbow
300 surgery / American Shoulder and Elbow Surgeons [et al]. 2018;27:160-6.
- 301 [17] Daggett M, Werner B, Collin P, Gauci MO, Chaoui J, Walch G. Correlation between glenoid
302 inclination and critical shoulder angle: a radiographic and computed tomography study. Journal of
303 shoulder and elbow surgery / American Shoulder and Elbow Surgeons [et al]. 2015;24:1948-53.
- 304 [18] Kandemir U, Allaire RB, Jolly JT, Debski RE, McMahon PJ. The relationship between the orientation
305 of the glenoid and tears of the rotator cuff. J Bone Joint Surg Br. 2006;88:1105-9.
- 306 [19] Nyffeler RW, Meyer DC. Acromion and glenoid shape: Why are they important predictive factors for
307 the future of our shoulders? EFORT Open Rev. 2017;2:141-50.
- 308 [20] Frich LH, Larsen MS. How to deal with a glenoid fracture. EFORT Open Rev. 2017;2:151-7.
- 309 [21] van Noort A, van der Werken C. The floating shoulder. Injury. 2006;37:218-27.

310 [22] Rasoulia A, Rohling R, Abolmaesumi P. Group-wise registration of point sets for statistical shape
311 models. IEEE transactions on medical imaging. 2012;31:2025-34.

312 [23] Styner MA, Rajamani KT, Nolte LP, Zsemlye G, Szekely G, Taylor CJ, et al. Evaluation of 3D
313 correspondence methods for model building. Information processing in medical imaging : proceedings
314 of the conference. 2003;18:63-75.

315 [24] Van Sint Jan S, Della Croce U. Identifying the location of human skeletal landmarks: why
316 standardized definitions are necessary--a proposal. Clinical biomechanics. 2005;20:659-60.

317 [25] Mutsvangwa T, Burdin V, Schwartz C, Roux C. An automated statistical shape model developmental
318 pipeline: application to the human scapula and humerus. IEEE transactions on bio-medical engineering.
319 2015;62:1098-107.

320 [26] Shrout PE, Fleiss JL. Intraclass correlations: uses in assessing rater reliability. Psychological bulletin.
321 1979;86:420-8.

322 [27] Goss TP. Fractures of Scapula: Diagnosis and treatment. In: Iannotti JP, Williams GR, editors.
323 Disorders of the shoulder: Diagnosis and Management. Philadelphia: Lippincott Williams & Wilkins;
324 1999. p. 597-637.

325 [28] Hardegger FH, Simpson LA, Weber BG. The operative treatment of scapular fractures. J Bone Joint
326 Surg Br. 1984;66:725-31.

327 [29] Besl PJ, McKay ND. A method for registration of 3-D shapes. IEEE transactions on pattern analysis
328 and machine intelligence. 1992;14:239-56.

329 [30] Lüthi M. SCALable Image analysis and Shape MOdelling. 2014.

330 [31] Lüthi M, Jud C, Vetter T. A Unified Approach to Shape Model Fitting and Non-rigid Registration.
331 Cham: Springer International Publishing; 2013. p. 66-73.

332 [32] Lüthi M, Gerig T, Jud C, Vetter T. Gaussian Process Morphable Models. IEEE transactions on pattern
333 analysis and machine intelligence. 2018;40:1860-73.

334 [33] Dubuisson M, Jain AK. A modified Hausdorff distance for object matching. Proceedings of 12th
335 International Conference on Pattern Recognition1994. p. 566-8 vol.1.

336 [34] Moor BK, Bouaicha S, Rothenfluh DA, Sukthankar A, Gerber C. Is there an association between the
337 individual anatomy of the scapula and the development of rotator cuff tears or osteoarthritis of the
338 glenohumeral joint?: A radiological study of the critical shoulder angle. Bone Joint J. 2013;95-B:935-41.

339 [35] Suter T, Gerber Popp A, Zhang Y, Zhang C, Tashjian RZ, Henninger HB. The influence of radiographic
340 viewing perspective and demographics on the critical shoulder angle. Journal of shoulder and elbow
341 surgery / American Shoulder and Elbow Surgeons [et al]. 2015;24:e149-58.

342 [36] Banas MP, Miller RJ, Totterman S. Relationship between the lateral acromion angle and rotator cuff
343 disease. *Journal of shoulder and elbow surgery / American Shoulder and Elbow Surgeons* [et al].
344 1995;4:454-61.

345 [37] Tuček M, Naňka O, Malík J, Bartoníček J. The scapular glenopolar angle: standard values and side
346 differences. *Skeletal radiology*. 2014;43:1583-7.

347 [38] Albrecht T, Luthi M, Gerig T, Vetter T. Posterior shape models. *Medical image analysis*. 2013;17:959-
348 73.

349 [39] Cole AK, McGrath ML, Harrington SE, Padua DA, Rucinski TJ, Prentice WE. Scapular bracing and
350 alteration of posture and muscle activity in overhead athletes with poor posture. *J Athl Train*.
351 2013;48:12-24.

352 [40] Romero J, Schai P, Imhoff AB. Scapular neck fracture--the influence of permanent malalignment of
353 the glenoid neck on clinical outcome. *Arch Orthop Trauma Surg*. 2001;121:313-6.

354

355

356

357

358

359

360

361

362

363

364

365

366

367

368

369 **Table 1:** Prediction error in the critical shoulder angle in terms of individual angle differences
 370 between angle obtained from the original shape and the angle predicted by each SSM type.

371

Anatomical Measure	Critical Shoulder Angle (°)								
	Scapula Name	Original Scapula	SSM _{non-augmented}	Prediction error	<i>a</i> SSM _{proposed}	Prediction error	<i>a</i> SSM _{set1}	Prediction error	<i>a</i> SSM _{set2}
Scap1	27.6	24.5	-3.1	26.0	-1.6	29.2	1.6	26.6	-1.0
Scap2	47.2	34.9	-12.3	35.9	-11.3	32.7	-14.5	33.1	-14.1
Scap3	27.7	32.7	5.0	28.4	0.7	29.0	1.3	28.3	0.6
Scap4	34.0	31.7	-2.3	32.7	-1.3	33.4	-0.6	31.9	-2.1
Scap5	36.6	33.5	-3.1	34.2	-2.4	33.1	-3.5	31.4	-5.2
Scap6	27.0	31.4	4.4	30.3	3.3	31.0	4.0	30.7	3.7
Mean Measure	33.35	31.45		31.25		31.40		30.33	
SD	7.17	3.32		3.39		1.80		2.22	
Absolute Mean Difference		5.03		3.43		4.25		4.45	
Min difference		2.30		0.70		0.60		0.60	
Max difference		12.30		11.30		14.50		14.10	

372

373

374

375

376

377
 378
 379
 380
 381
 382
 383
 384
 385

Table 2: Prediction error in the glenoid inclination angle in terms of individual angle differences between angle obtained from the original shape and the angle predicted by each SSM type.

Anatomical Measure	Glenoid inclination (°)								
	Scapula Name	Original Scapula	SSM _{non-augmented}	Prediction error	α SSM _{proposed}	Prediction error	α SSM _{set1}	Prediction error	α SSM _{set2}
Scap1	68.0	73.7	5.7	71.0	3.0	69.0	1.0	71.3	3.3
Scap2	80.5	83.8	3.3	79.5	-1.0	83.6	3.1	83.3	2.8
Scap3	72.5	71.7	-0.8	73.0	0.5	74.4	1.9	78.9	6.4
Scap4	70.6	67.6	-3.0	74.6	4.0	79.8	9.2	80.3	9.7
Scap5	69.1	70.3	1.2	74.7	5.6	73.6	4.5	76.5	7.4
Scap6	73.6	71.8	-1.8	74.8	1.2	76.6	3.0	84.0	10.4
Mean Measure	72.38	73.15		74.60		76.17		79.05	
SD	4.09	5.11		2.57		4.65		4.30	
Absolute Mean Difference		2.63		2.55		3.78		6.67	
Min difference		0.80		0.50		1.00		2.80	
Max difference		5.70		5.60		9.20		10.40	

386
 387
 388
 389
 390

391
 392
 393
 394
 395
 396
 397
 398
 399
 400

Table 3: Prediction error in the lateral acromion angle in terms of individual angle differences between angle obtained from the original shape and the angle predicted by each SSM type.

Anatomical Measure	Lateral acromion angle (°)									
	Scapula Name	Original Scapula	<i>SSM_{non-augmented}</i>	Prediction error	<i>aSSM_{proposed}</i>	Prediction error	<i>aSSM_{set1}</i>	Prediction error	<i>aSSM_{set2}</i>	Prediction error
	Scap1	93.8	99.9	6.1	87.0	-6.8	88.2	-5.6	100.0	6.2
	Scap2	82.2	86.7	4.5	84.6	2.4	87.1	4.9	88.8	6.6
	Scap3	76.6	81.3	4.7	80.2	3.6	86.5	9.9	86.9	10.3
	Scap4	76.1	81.8	5.7	78.6	2.5	81.5	5.4	85.1	9.0
	Scap5	85.5	82.2	-3.3	87.1	1.6	88.3	2.8	83.6	-1.9
	Scap6	89.1	83.7	-5.4	86.4	-2.7	83.3	-5.8	87.9	-1.2
Mean Measure		83.88	85.93		83.98		85.82		88.72	
SD		6.39	6.50		3.37		2.55		5.33	
Absolute Mean Difference			4.95		3.27		5.73		5.87	
Min difference			3.30		1.60		2.80		1.20	
Max difference			6.10		6.80		9.90		10.30	

401
 402
 403
 404

405
 406
 407
 408
 409
 410
 411
 412
 413

Table 4: Prediction error in the glenopolar angle in terms of individual angle differences between angle obtained from the original shape and the angle predicted by each SSM type.

Anatomical Measure	Glenopolar angle (°)									
	Original Scapula	<i>SSM_{non-augmented}</i>	Prediction error	<i>aSSM_{proposed}</i>	Prediction error	<i>aSSM_{set1}</i>	Prediction error	<i>aSSM_{set2}</i>	Prediction error	
Scap1	36.6	37.5	0.9	34.5	-2.1	38.2	1.6	34.9	-1.7	
Scap2	47.4	42.4	-5.0	42.2	-5.2	37.7	-9.7	37.8	-9.6	
Scap3	39.2	38.8	-0.4	36.9	-2.3	36.9	-2.3	32.8	-6.4	
Scap4	44.2	44.1	-0.1	38.0	-6.2	34.4	-9.8	32.6	-11.6	
Scap5	43.6	41.4	-2.2	36.1	-7.5	39.3	-4.3	35.7	-7.9	
Scap6	39.5	39	-0.5	36.2	-3.3	34.8	-4.7	29.4	-10.1	
Mean Measure	41.75	40.53		37.32		36.88		33.87		
SD	3.64	2.29		2.42		1.77		2.66		
Absolute Mean Difference		1.52		4.43		5.40		7.88		
Min difference		0.10		2.10		1.60		1.70		
Max difference		5.00		7.50		9.80		11.60		

414
 415
 416
 417
 418

419 **FIGURE LEGENDS**

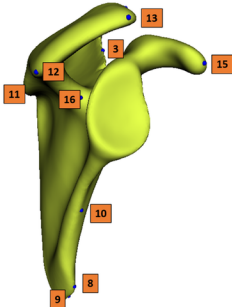
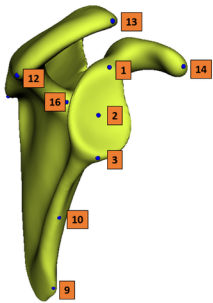
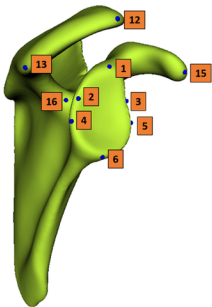
420 **Figure 1: Three landmark sets used for augmenting the scapula SSM.** Each landmark set
421 contains 16 anatomically placed landmarks. First column shows proposed landmark set with six
422 landmarks mapping the glenoid cavity and four mapping the acromion. Second column shows
423 Set1 landmarks with three landmarks mapping the glenoid cavity and rest of them mapping the
424 scapular edges. Third column shows Set2 landmarks with no landmarks in the glenoid cavity
425 region.

426

427 **Figure 2: Sample goodness of fit in the glenoid region for three augmented SSMs.** Red color
428 indicates original shape while the transparent green color indicates predicted shape after
429 performing one-time non-rigid deformation for each augmented SSM. Two views for each fit are
430 shown for each fitting where: A) Fitting result for $aSSM_{\text{proposed}}$, B) Fitting results for $aSSM_{\text{set1}}$,
431 and C) Fitting results for $aSSM_{\text{set2}}$.

432

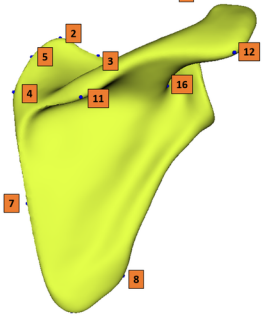
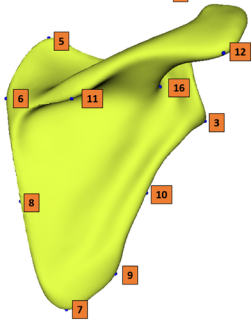
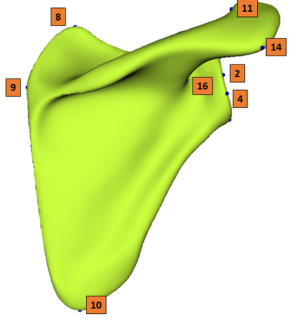
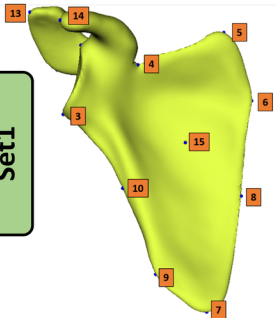
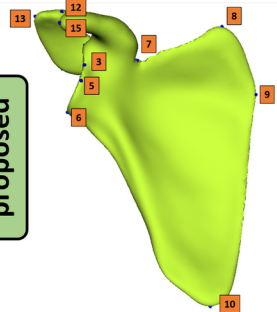
433 **Figure 3: Comparing the four SSMs (non-augmented SSM, augmented SSM proposed,**
434 **augmented SSM set1, and augmented SSM set2) for their fitting quality to predict the**
435 **glenoid region.** The graph shows the performance of each SSM type quantified using the mean
436 measures of distance and similarity from six external scapulae. Error bars on each column
437 indicate +/-1 SD from the mean value. Significance was established when $p \leq 0.05$ and indicated
438 using * above the bar graph. RMS: Root Mean Square distance, Hausdorff: Hausdorff distance
439 metric used to report maximum distance between original and predicted shapes [33].

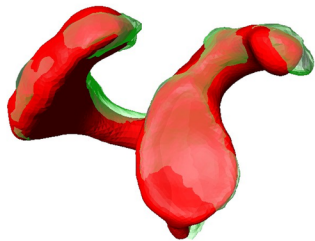
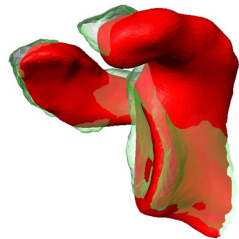
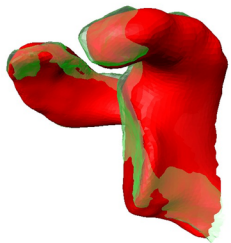


proposed

Set1

Set 2

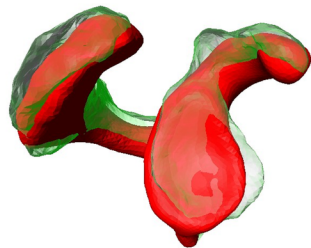




A



B



C

